



## Research Article

# Inelastic input energy spectra of far-fault ground motions: influence of hysteresis model

Onur MERTER<sup>1</sup>, Taner UCAR<sup>2,\*</sup>

<sup>1</sup>Izmir University of Economics, Department of Civil Engineering, Izmir, Türkiye

<sup>2</sup>Dokuz Eylül University, Department of Architecture, Izmir, Türkiye

## ARTICLE INFO

### Article history

Received: 05 February 2021

Accepted: 29 May 2021

### Keywords:

Energy equivalent velocity;  
Far-fault ground motions;  
Input energy spectra; Hysteresis  
model; Time history analysis

## ABSTRACT

The main purpose of the present study is to compute the input energy spectra of selected far-fault ground motions (GMs) for linear elastic systems, and inelastic systems having a constant ductility ratio. Elastic-perfectly plastic (EPP) and Modified Takeda hysteresis models have been adopted in nonlinear modeling of single-degree-of-freedom (SDOF) systems. Accelerograms of far-fault GMs have been compiled from the Pacific Earthquake Research Center (PEER) database. Linear and nonlinear time history analyses have been performed using the selected GMs records for SDOF systems having a damping ratio of 5%. Input energy spectral ordinates have been computed in terms of energy equivalent velocity. The results have shown that there is no significant difference between elastic and inelastic input energy spectral values at intermediate and long periods. However, for short period systems, input energy demand imposed on inelastic systems is generally greater than that of imposed on elastic systems. For short period systems, it can be inferred from the computations of the study that the input energy spectral values obtained using Modified Takeda hysteresis model are greater than those of other models that have been employed. However, input energy spectra for inelastic systems have no significant dependency on hysteresis models, especially for intermediate and long period systems.

**Cite this article as:** Merter O, Ucar T. Inelastic input energy spectra of far-fault ground motions: influence of hysteresis model. Sigma J Eng Nat Sci 2022;40(3):593–609.

## INTRODUCTION

Seismic design of structures is commonly based on strength- or force-based methods, despite their shortcomings, to achieve the life safety objective. Strength-based analysis methods in many seismic design codes and

standards such as Uniform Building Code [1], Eurocode 8 [2], National Building Code of Canada [3], International Building Code [4], Minimum Design Loads for Buildings and Other Structures [5] and Turkey Building Earthquake

\*Corresponding author.

\*E-mail address: [taner.ucar@deu.edu.tr](mailto:taner.ucar@deu.edu.tr)

This paper was recommended for publication in revised form by  
Regional Editor Abdelraheem Mahmoud Aly



Code [6] generally take into consideration the strength capacity of structural members. Strong ground motion (GM) effect is generally considered as equivalent static lateral loads in traditional code-based seismic design procedures. Earthquake (EQ) demand is defined in the form of acceleration response spectra, which are the plots of peak responses of all possible SDOF systems. In strength-based design philosophy, force levels are computed based on elastic stiffness and somewhat arbitrary force reduction factors are used to consider the nonlinear behaviour indirectly [7].

It has been further realized that strength is important but only in that it helps to reduce displacements, as well as strains, both of which can be directly related to structural damage. Accordingly, it is not possible to correlate exactly the nonlinear behaviour and structural performance with strength. Therefore, to relate structural damage to deformations, direct displacement-based design (DDBD) philosophy using displacements as the basis for the seismic design is proposed by Priestley et al. [8]. The main idea of the DDBD is to design structural systems according to an acceptable level of damage under GM effects.

However, both traditional strength-based and displacement-based procedures ignore the effects such as EQ duration, frequency content, and hysteretic behaviour. However, energy parameters involve these concepts and so they have gained great attention in seismic design in the last few decades [9]. More clearly, one of the most emerging developments in seismic design has been increased emphasis on energy-based design based on widely-accepted consideration that seismic energy concepts clarify the structural behaviour more rational under seismic effects [10-14]. In seismic design, the use of the energy concept was first proposed by Housner [15] and many different researchers used energy principles in earthquake-resistant structural design after then. Seismic input energy was researched and equations were proposed for the energy input [10, 13, 16-27]. Calculation of seismic input energy plays an important role in energy-based structural design. The determination of the energy dissipation in structural members by the elastic and inelastic behaviour depends on the knowledge of seismic input energy [28]. In the short period range of systems, the seismic input energy is a stable quantity and it is governed primarily by the natural period and mass [22]. For this reason, EQ input energy spectra have become effective tools to determine the energy input to SDOF systems. The input energy spectra cover characteristics of GMs and structural system, and they can be computed for both elastic and inelastic SDOF systems [13, 29].

In developing an energy-based design approach, the earthquake input energy should be properly defined preliminarily. In addition to characteristics of GMs, the earthquake input energy is closely associated with the velocity response of the system and each system parameters affecting the velocity response of the mass (i.e., natural period,

damping ratio of the system, yield deformation, and force-deformation relation) will likely affect the input energy response of the system. Accordingly, the present study focuses on the last one and the main objective of the study is to develop input energy spectra for inelastic systems represented by two common hysteresis models employed for reinforced concrete and steel structures.

A set of nine real earthquake ground motion (EQGM) records have been selected from PEER database. All accelerograms have been obtained from the records in far-fault regions and in other words, far-fault ground motions, having shortest distances from the station to the fault rupture surface of more than 20 km, have been considered. Linear and nonlinear time history analyses have been performed using selected far-fault EQs for SDOF systems having a damping ratio of 5%. Input energy spectra of selected far-fault EQGMs have been computed using the Excel program developed by the Authors. Both linear elastic and inelastic SDOF systems have been used for analyses. Displacement ductility ratio has been selected as  $\mu = 4$ , for inelastic systems, and EPP and Modified Takeda hysteresis models have been considered in nonlinear analyses. Elastic and inelastic input energy values have been computed in terms of energy equivalent velocity ( $V_{eq}$ ) and consequently, spectral ordinates have been obtained in terms of  $V_{eq}$ . Moreover, input energy per unit mass spectral values are also computed for elastic and inelastic SDOF systems. The variation of elastic and inelastic input energy spectral values and the influence of the hysteresis model on the input energy spectrum are investigated. The results have shown that the far-fault input energy spectra have some dependency on the hysteresis model specifically along some period ranges. The hysteresis model influences the inelastic input energy spectra of GMs, especially at short period ranges. The outcomes of the study are quite important since they clarify the variation of input energy with the hysteresis model for commonly encountered systems.

## INPUT ENERGY EXPRESSION AND ENERGY SPECTRUM CONCEPT

Energy-based seismic design concept and energy-related design parameters were first formulated for SDOF systems. The general equation of motion can be written for the lumped-mass inelastic SDOF system, which is subjected to an EQ excitation as [30]:

$$m \cdot \ddot{u} + c \cdot \dot{u} + f_s(u) = -m \cdot \ddot{u}_g(t) \quad (1)$$

where  $u$  is the relative displacement with respect to ground,  $m$  is the mass,  $\dot{u}$  is the velocity of the mass,  $\ddot{u}$  is the acceleration of the mass,  $c$  is the coefficient of viscous damping,  $f_s(u)$  is the resisting force and  $\ddot{u}_g(t)$  is the ground acceleration. Energy parameters may be expressed by integrating Eq. (1) over the relative displacement:

$$\int_0^{u(t)} m \cdot \ddot{u} du + \int_0^{u(t)} c \cdot \dot{u} du + \int_0^{u(t)} f_s(u) du = - \int_0^{u(t)} m \cdot \ddot{u}_g(t) du \quad (2)$$

Eq. (2) is called the energy balance equation of a SDOF system. It can be turned into a time integral as:

$$\int_0^t m \cdot \ddot{u} \cdot \dot{u} dt + \int_0^t c \cdot \dot{u}^2 dt + \int_0^t f_s(u) \cdot \dot{u} dt = - \int_0^t m \cdot \ddot{u}_g(t) \cdot \dot{u} dt \quad (3)$$

where  $du = \dot{u} dt$  ( $t$  shows the entire duration of EQ). Eq. (3) is the time integral version of the general energy balance equality and it can be rewritten in terms of representative energy components as:

$$E_K + E_\xi + [E_{Se} + E_H] = E_I \quad (4)$$

where  $E_K$ ,  $E_\xi$ ,  $E_{Se}$  and  $E_H$  represent the kinetic energy, damping energy, elastic strain energy and hysteretic energy, respectively.  $E_I$  represents the total seismic energy input to the system with GM effect. In Eq. (3),  $E_K$  corresponds to the first integral term,  $E_\xi$  corresponds to the second integral term and the total of  $E_{Se}$  and  $E_H$  (the total absorbed energy by the structure) corresponds to the third integral term. Hysteretic energy ( $E_H$ ) is generally referred to as the most important energy component and it is associated with structural damage in scientific researches [19, 29, 31, 32]. The total seismic input energy ( $E_I$ ) can be obtained from the right-hand side of Eq. (3) as:

$$E_I = - \int_0^t m \cdot \ddot{u}_g(t) \cdot \dot{u} dt \quad (5)$$

It is quite evident from Eq. (5) that the input energy per unit mass ( $E_I/m$ ) can be written as:

$$E_I/m = - \int_0^t \ddot{u}_g(t) \cdot \dot{u} dt \quad (6)$$

The seismic input energy can be computed both for elastic and inelastic systems. If the system is linearly elastic, then the energy term  $\int_0^t f_s(u) \cdot \dot{u} dt$  can be written as  $\int_0^t (k \cdot u) \cdot \dot{u} dt$ , where  $k$  represents the lateral stiffness of the system. However, if the system is inelastic then the force  $f_s(u)$  can be interpreted as nonlinear resisting force and it depends upon the time history of displacement and velocity [30]. When the structural system behaves nonlinear, then the computed input energy is referred to as inelastic input energy.

Once the input energy time history is computed for a damped SDOF system under EQGM effect, then the maximum input energy value can be readily obtained. The maximum seismic input energy can be expressed without

depending on the mass of the system, as can be seen from Eq. (6). The graph of  $E_I/m$  versus  $T_n$  (the natural vibration period of the system) can be plotted and this diagram is called the input energy spectrum. In the input energy spectrum graph, the maximum input energy values corresponding to different natural vibration periods are combined into a single graph. The development of the input energy spectrum can be seen in Figure 1. In addition to characteristics of seismic input, inelastic input energy spectrum is a function of natural vibration period ( $T_n$ ), damping ratio ( $\xi$ ), yield deformation ( $u_y$ ), and hysteresis model, since the velocity response of the inelastic SDOF system depends on these structural parameters [33]. Accordingly, this dependence on structural parameters can be written as in Eq. (7). It is clear that the last two parameters are eliminated in case of elastic input energy spectrum.

$$E_I = E_I(T_n, \xi, u_y, f_s(u)) \quad (7)$$

### SELECTED GMS

The EQ data of the present study includes processed ordinary (nonpulse-like) GM records which are recorded at closest fault distances not less than 30 km. The data consists of a set of nine far-fault real GMS which are all compiled from PEER NGA-West2 strong GM database [34]. Selected accelerograms are presented in Figure 2. Joyner-Boore distances ( $R_{JB}$ ) are in the range of 35-121 km. Focal mechanism is strike-slip. The moment magnitudes ( $M_w$ ) of EQs range from 6.19 to 7.2 and shear wave velocities of the upper 30 meters of the soil profile ( $V_{s30}$ ) are between 180 and 360 m/s (soil site class D according to NEHRP site classification). The peak ground accelerations (PGA) are between 0.040g and 0.151g, the peak ground velocities (PGV) are between 2.91 and 14.16 cm/s and the peak ground displacements (PGD) are between 0.50 and 16.34 cm. The characteristics of the selected far-fault EQGMS are given in Table 1, where  $I_A$  is the Arias Intensity.

### CONSIDERED HYSTERESIS MODELS AND TIME HISTORY ANALYSES

Two basic hysteresis models that are commonly employed in EQ engineering, elastic-perfectly plastic (EPP) and Modified Takeda hysteresis models, were considered to represent the hysteretic behaviour of SDOF systems within the study. In Figure 4, the set of rules which define force-displacement relations of the employed hysteresis models can be seen. These models define a nonlinear hysteretic relation between the force ( $F$ ) and the displacement ( $u$ ). EPP model is usually used for representing the hysteretic behaviour of steel structures under EQGM induced loading reversals, whereas Modified Takeda model is employed for reinforced concrete structures. Accordingly, the analyses of

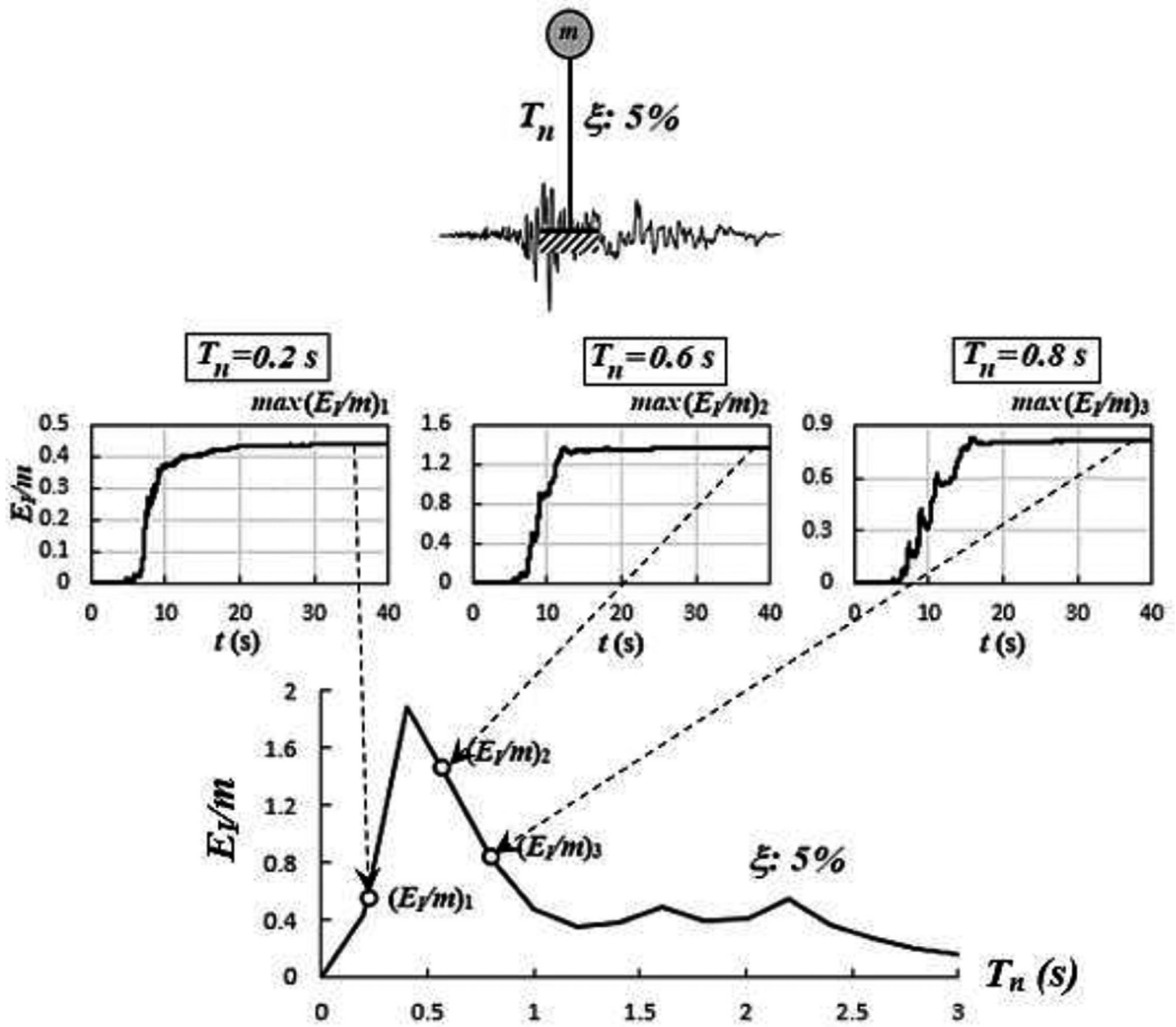


Figure 1. Construction of input energy spectrum.

Table 1. Selected far-fault EQGMs

#EQ	Event Name	Station	Year	$M_w$	$I_A$ (m/s)	$R_{JB}$ (km)	$V_{s30}$ (m/s)	PGA (g)	PGV (cm/s)	PGD (cm)
1	Trinidad	Rio Dell Overpass	1980	7.2	0.39	76.06	311.75	0.151	8.87	3.60
2	Northw. Calif-02	Ferndale City Hall	1941	6.6	0.03	91.15	219.31	0.040	3.42	1.12
3	Northern Calif-01	Ferndale City Hall	1941	6.4	0.10	44.52	219.31	0.122	6.77	1.33
4	El Alamo	El Centro Array #9	1956	6.8	0.10	121	213.44	0.051	7.08	4.09
5	Imp. Valley-06	Niland Fire Station	1979	6.53	0.11	35.64	212.00	0.069	8.58	5.17
6	Victoria_ Mexico	SAHOP Casa Flores	1980	6.33	0.08	39.1	259.59	0.069	8.94	2.19
7	Morgan Hill	Capitola	1984	6.19	0.23	39.08	288.62	0.142	8.29	1.68
8	Morgan Hill	Los Banos	1984	6.19	0.05	63.16	262.05	0.062	9.17	2.27
9	Morgan Hill	SF Intern. Airport	1984	6.19	0.04	70.93	190.14	0.048	2.91	0.50

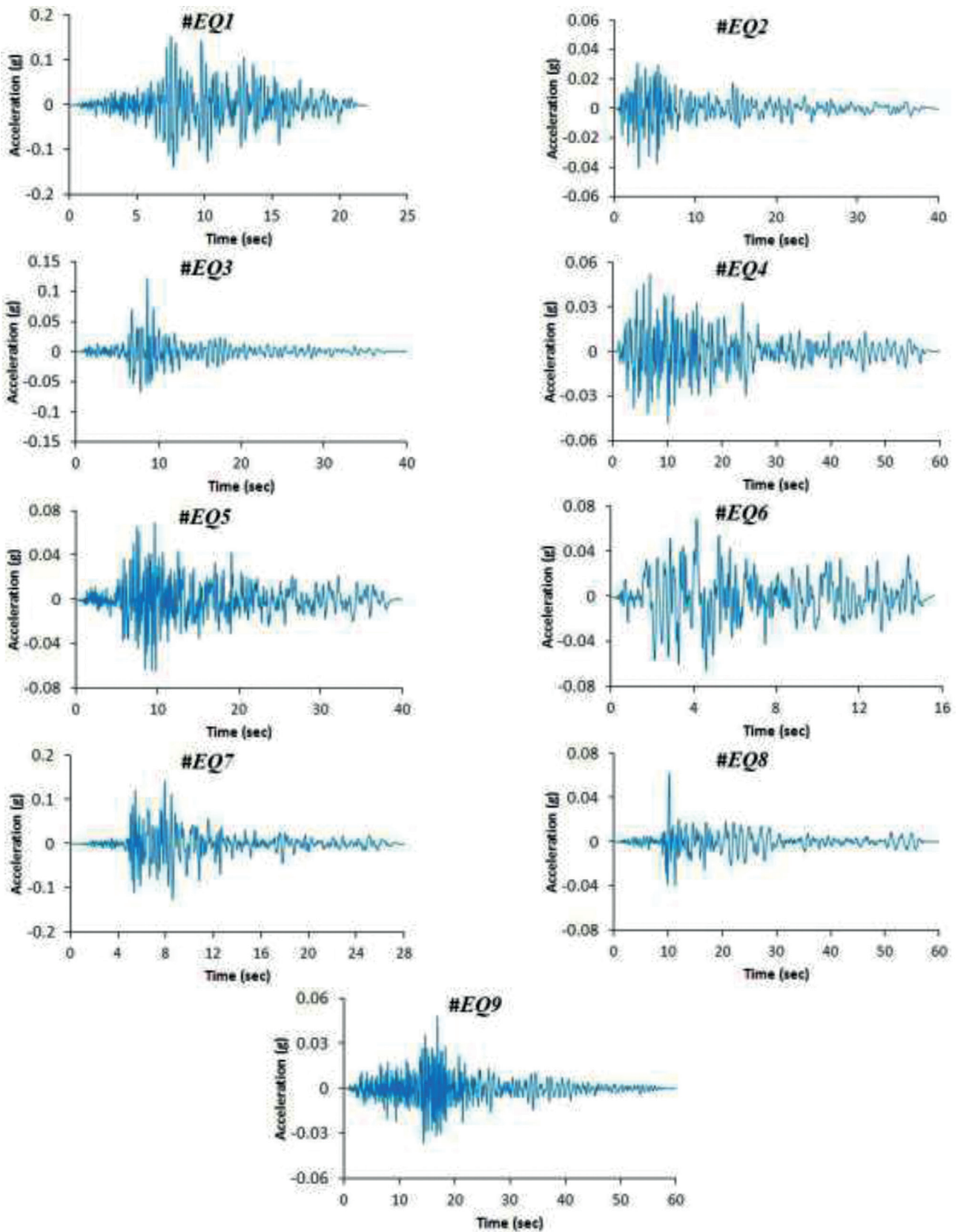


Figure 2. Acceleration time histories.

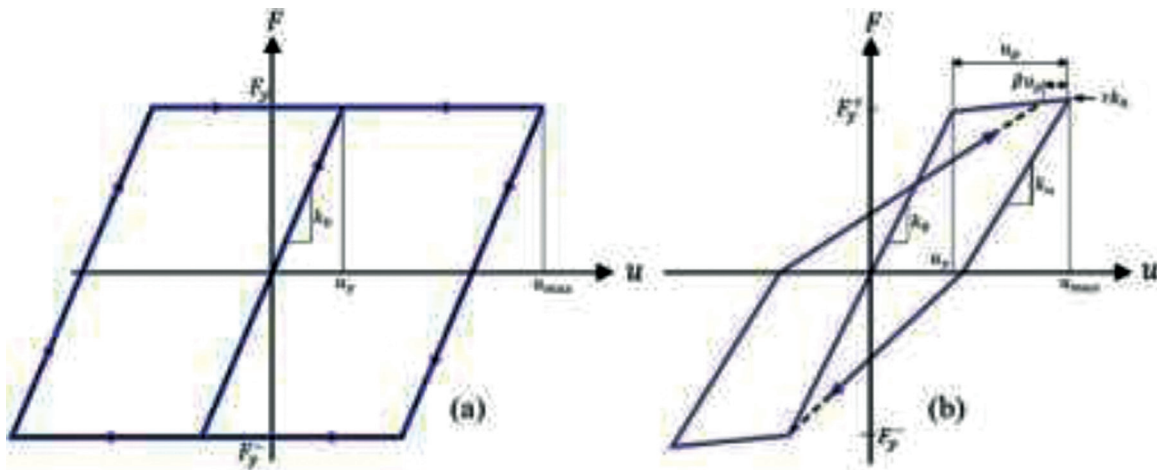


Figure 3. a) Elastic-perfectly plastic (EPP) and b) Modified Takeda hysteresis models.

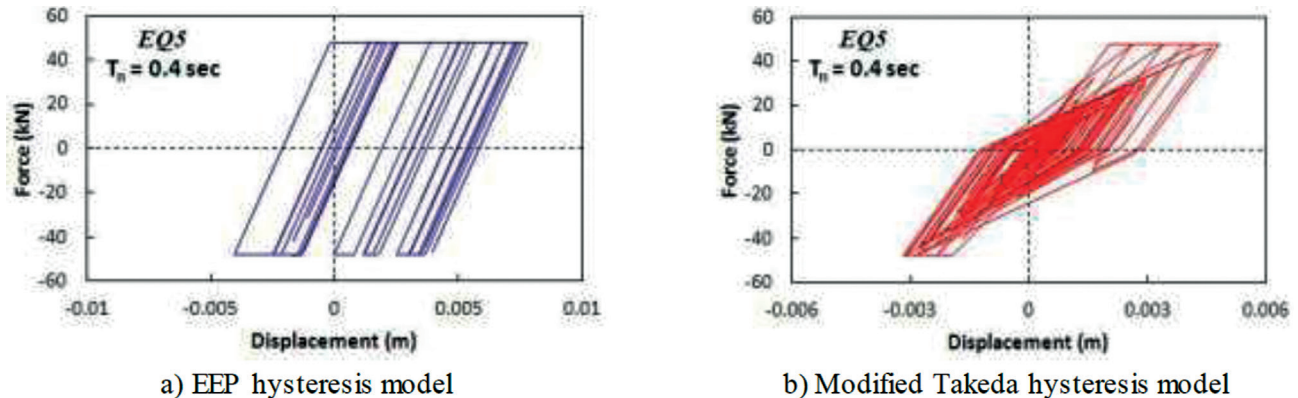


Figure 4. Hysteresis relations of SDOF system.

the present study may be regarded to represent some analytical results for the two most common types of structures. In Figure 3 (a),  $F_y$  shows the yield force,  $u_y$  is the yield displacement,  $u_{max}$  is the maximum displacement and  $k_o$  is the lateral stiffness. Additionally, for Takeda hysteresis model in Figure 3 (b),  $r$  is the post-yield stiffness factor,  $\beta$  shows the reloading stiffness factor,  $k_o$  is the initial lateral stiffness,  $k_u$  is the unloading stiffness and  $u_p$  shows the plastic displacement [35, 36].

Dynamic time history analyses were performed for linear elastic and nonlinear SDOF systems utilizing the software PRISM [37], which uses Newmark time integration method for the solution of second-order ordinary differential equation of motion. The post-yield stiffness factor ( $r$ ) is considered as 0 in Modified Takeda hysteresis model. Time history analyses were performed for SDOF systems having a damping ratio of 5% using the selected accelerograms. For EQ5, EPP and Modified Takeda hysteresis relations ( $F-u$  relations) of SDOF system having period of  $T_n = 0.4$  sec is shown in Figure 4.

In the study, velocity time histories ( $\dot{u}-t$  relations) of SDOF system were computed using the selected far-fault EQGMs in Table 1. After computing velocity time histories by PRISM software, seismic input energy histories for different natural periods of vibration were obtained by using the Excel program developed by the authors. Then the input energy spectra of selected GMs were expressed in terms of  $V_{eq}$  as:

$$V_{eq} = \sqrt{2E_1/m} \quad (8)$$

The developed algorithm and the successive steps utilized in computing energy equivalent velocity spectra are summarized in the flowchart of Figure 5.

## DISCUSSION AND RESULTS

### Input energy spectra of far-fault GMs

In Figure 6, elastic input energy spectra, as well as inelastic input energy spectra based on EPP and Modified

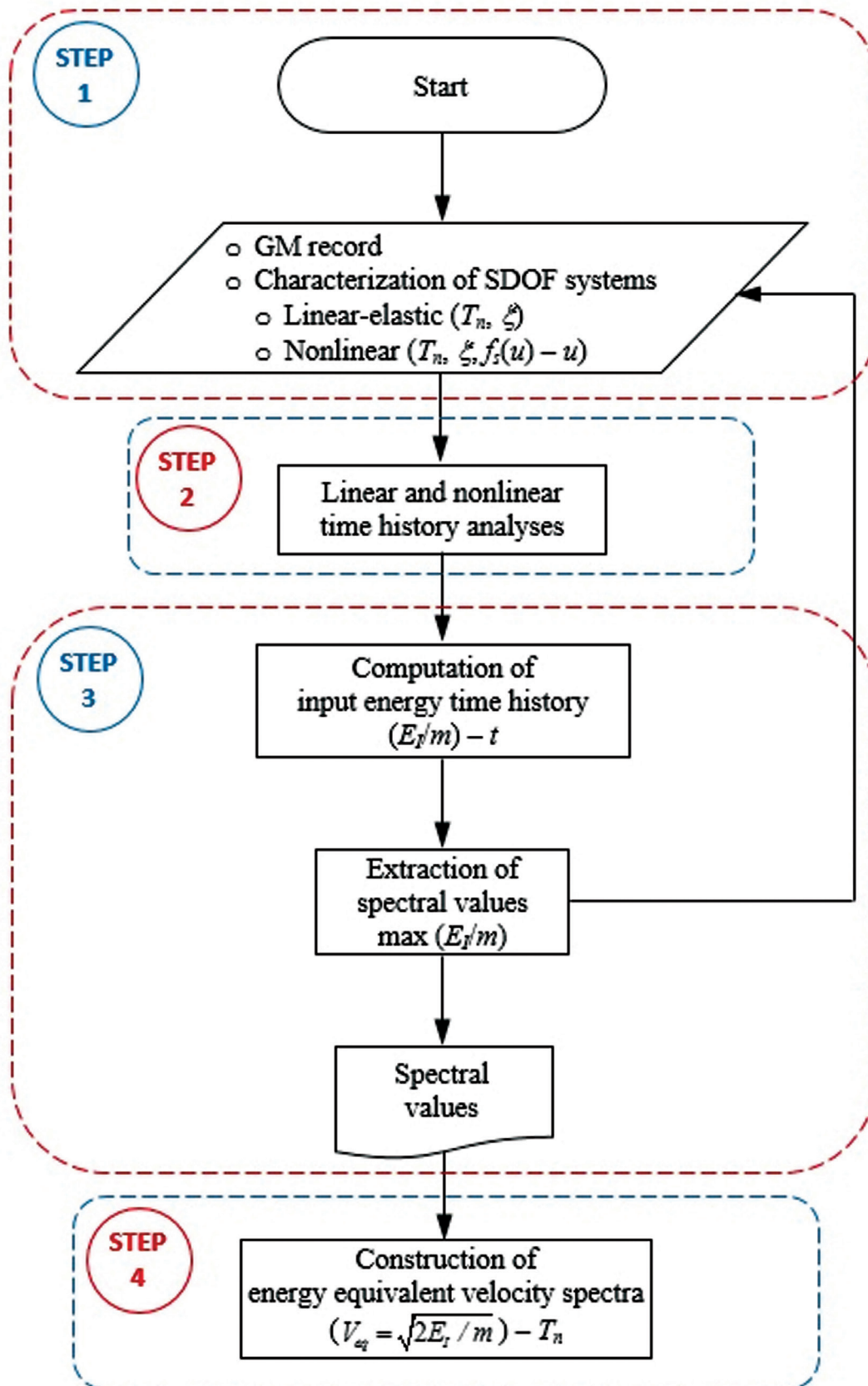


Figure 5. Flowchart for computing energy equivalent velocity spectra.

Takeda hysteresis models, are presented for EQ1, EQ2 and EQ3. The variation of input energy spectra  $V_{eq}$  with different hysteretic models is presented for EQ4, EQ5 and EQ6 in Figure 7. The energy spectrum of the last group GMs is presented in Figure 8. A constant displacement ductility ratio of  $\mu = 4$  is considered for inelastic models. It can be observed from those figures that elastic and inelastic input spectra of far-field GMs are somewhat different and hysteresis model has some influence on inelastic input spectra. Although some other trends can be observed from input energy spectra of individual GM records, they are quite jagged, and forthcoming observations will therefore be based on a set of smooth spectra.

Before developing smooth input energy spectra,  $V_{eq}$  spectral ordinates for some specific periods are plotted in Figure 9 in order to make clear the dependency of input energy spectral values on GM characteristics and structural properties. It is quite obvious that even subjected to the same GM, different input energy demands are imposed on SDOF systems based on their natural periods. The variation of input energy spectral values with EQ number clarifies that each GM reflects its own characteristic in input energy computations.

Smoother spectral curves can be plotted based on mean  $V_{eq}$  spectral ordinates. In Figure 10 (a), input energy spectra of the considered GMs is obtained as the arithmetic mean of spectral ordinates computed for individual

records, whereas geometric mean of  $V_{eq}$  spectral ordinates of individual records is used in computing input spectra in Figure 10 (b). It can be clearly observed from Figure 10 input energy demand imposed on inelastic systems is greater than that of elastic systems at short periods ( $T_n < 0.5$  sec). For systems in acceleration-sensitive region of the spectrum, the peak deformation of inelastic system is larger than the peak deformation of the elastic system, which in turn leads to greater input energy demands in that spectral region. Starting from a certain period around 0.5-0.6 sec, elastic input energy becomes higher than inelastic input spectra at intermediate and long periods. On the other hand, far-fault input energy spectra have some dependency on hysteresis model along the entire period range, but it seems that inelastic input spectra based on EEP hysteresis model is very close to elastic input spectra at long periods.

Variation of inelastic to elastic input energy spectral values with natural period is plotted in Figure 11 for each GM record. Higher input energy demands are imposed on inelastic systems with short period ( $T < 0.5$  sec). The spectral ratios oscillating around unity imply that elastic and inelastic input energy spectral ordinates are very close to each other.

Variation of the arithmetic mean of inelastic to elastic input energy spectral ordinates with the natural period is presented in Figure 12 (a). It can be clearly observed from Figure 12 (a) that for both hysteresis models inelastic

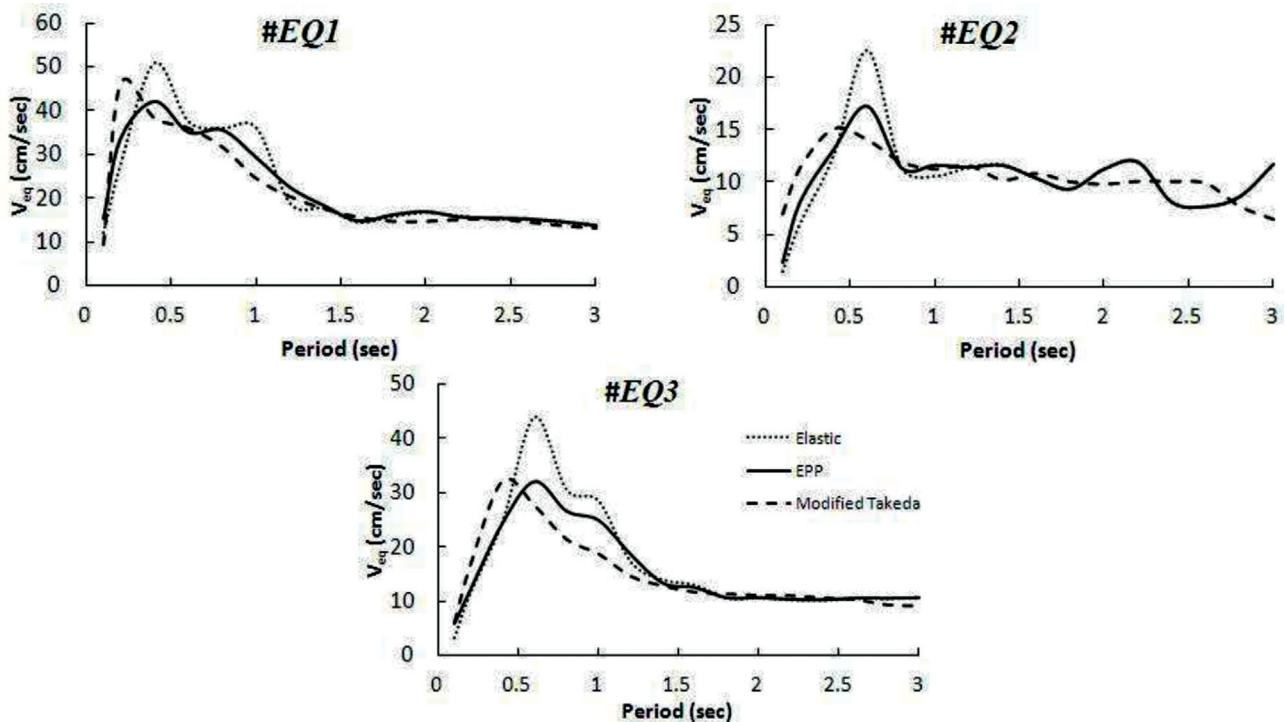


Figure 6. 5% damped elastic and inelastic  $V_{eq}$  spectra of EQ1, EQ2 and EQ3.

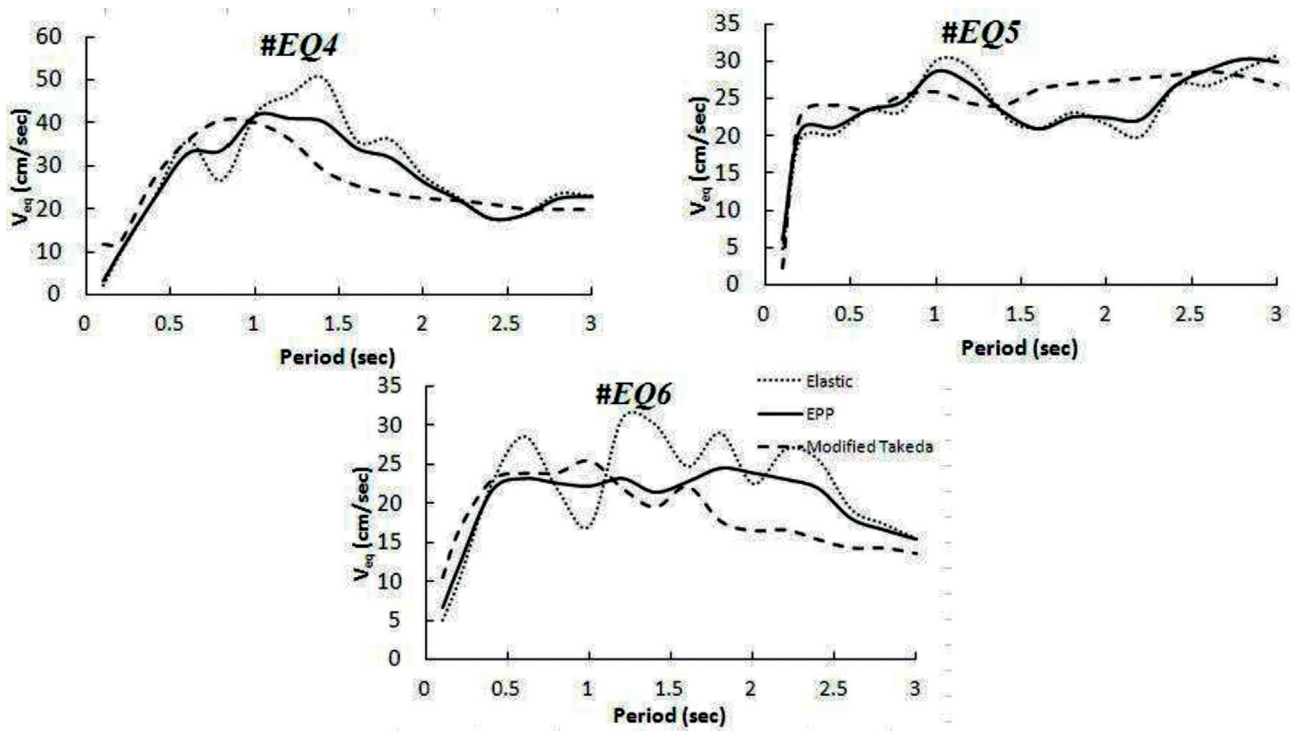


Figure 7. 5% damped elastic and inelastic  $V_{eq}$  spectra of EQ4, EQ5 and EQ6.

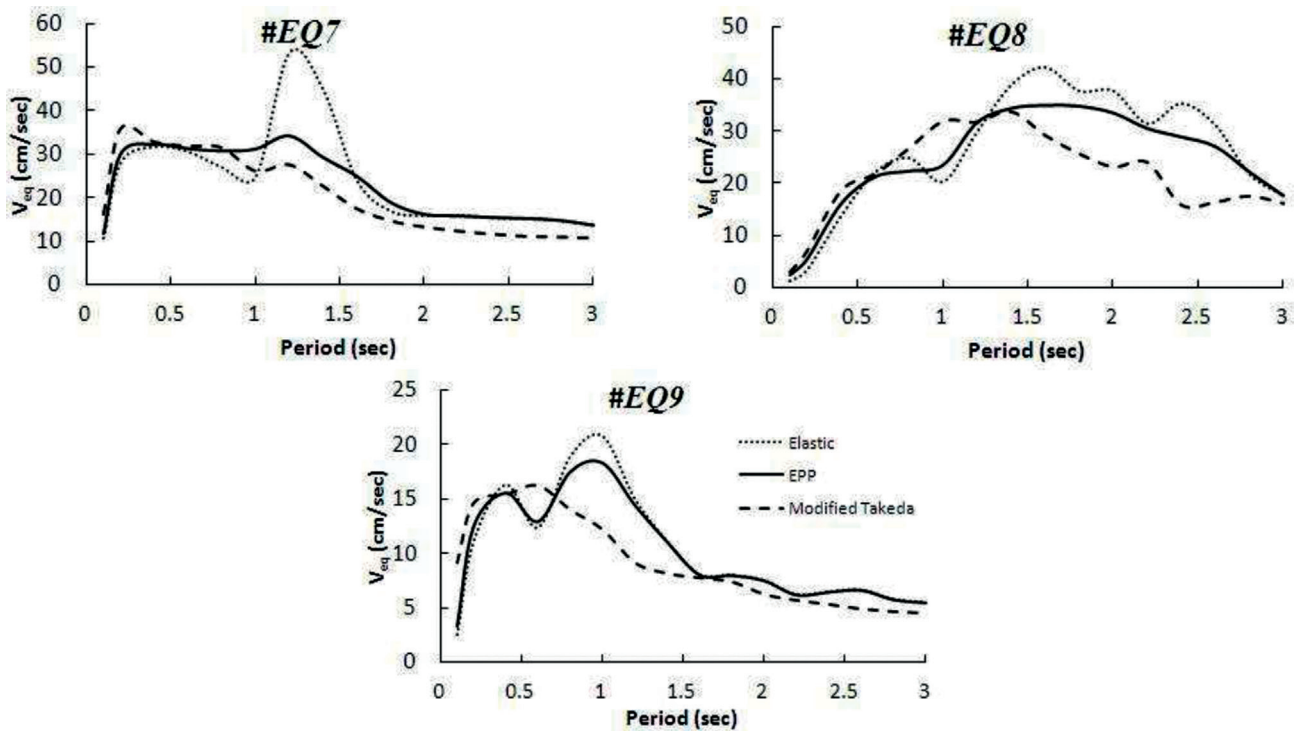


Figure 8. 5% damped elastic and inelastic  $V_{eq}$  spectra of EQ7, EQ8 and EQ9.

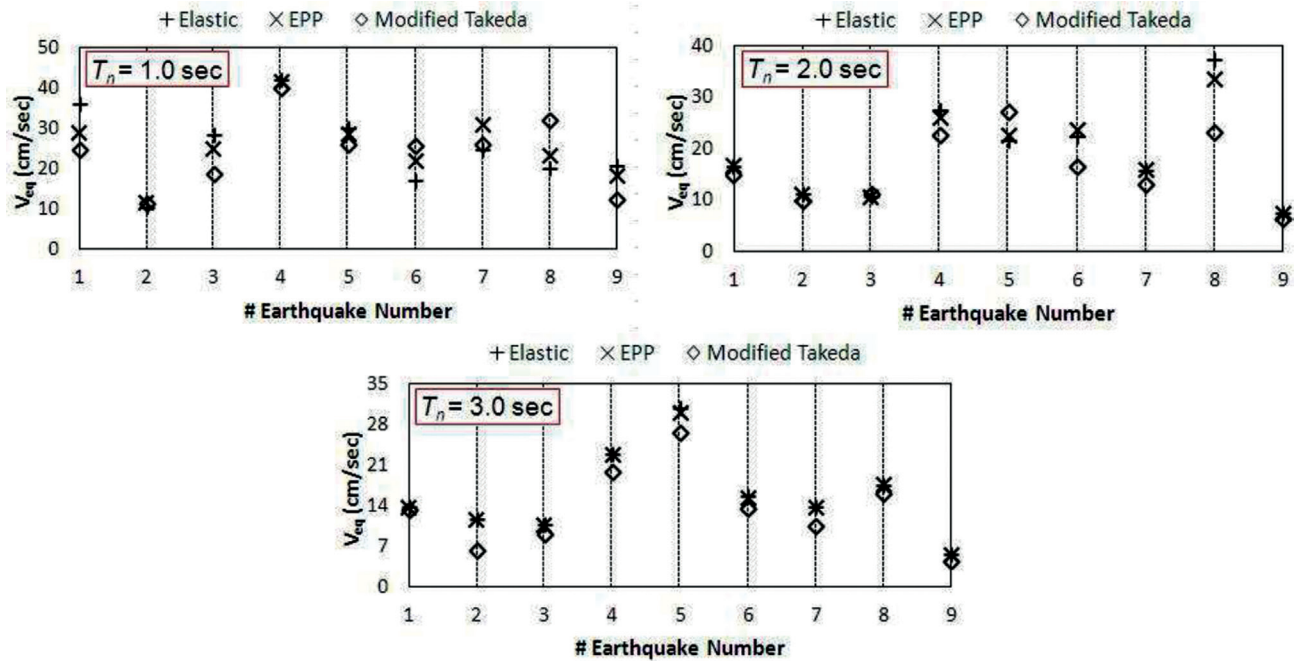


Figure 9.  $V_{eq}$  spectral ordinates of the selected EQs at periods of 1.0, 2.0 and 3.0 sec.

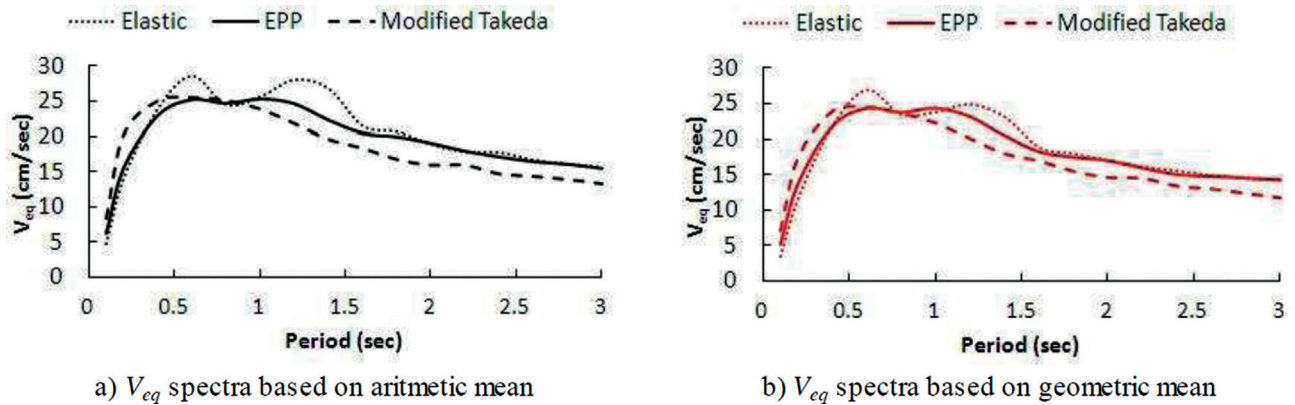


Figure 10. Smooth  $V_{eq}$  spectra.

input energy spectral ordinates are greater than those of elastic input energy spectra. In fact, inelastic input energy is higher than elastic input energy below a certain period around 0.5–0.6 sec. Therefore, elastic input energy constitutes a lower bound to inelastic input energy for periods less than 0.5–0.6 sec. On the contrary, at longer periods the mean elastic input energy spectrum is higher than the inelastic one. Those results of the present study are consistent with those of Alici and Sucuoğlu [38] and Ucar [39], which are conducted for near-fault GMs, as well as of Decanini and Mollaioli [40] which considers both near- and far-fault GMs. In addition, at short periods hysteresis model is found to be influential on inelastic input energy spectral values. At longer periods,

input energy spectra for EPP systems to elastic systems oscillate around unity, which implies that input energy demands on EPP systems, are almost identical to elastic systems. However, input energy spectral values computed by employing Modified Takeda hysteresis model are somewhat lower than those of elastic systems, at longer periods.

Figure 12 (b) shows the ratio of mean inelastic input energy spectral values computed by employing EPP and Modified Takeda hysteresis models. At short periods, input energy spectra computed using Modified Takeda hysteresis model is found to be higher than those of EPP hysteresis model. On the contrary, input energy spectral ordinates computed for inelastic SDOF systems simulated by EPP

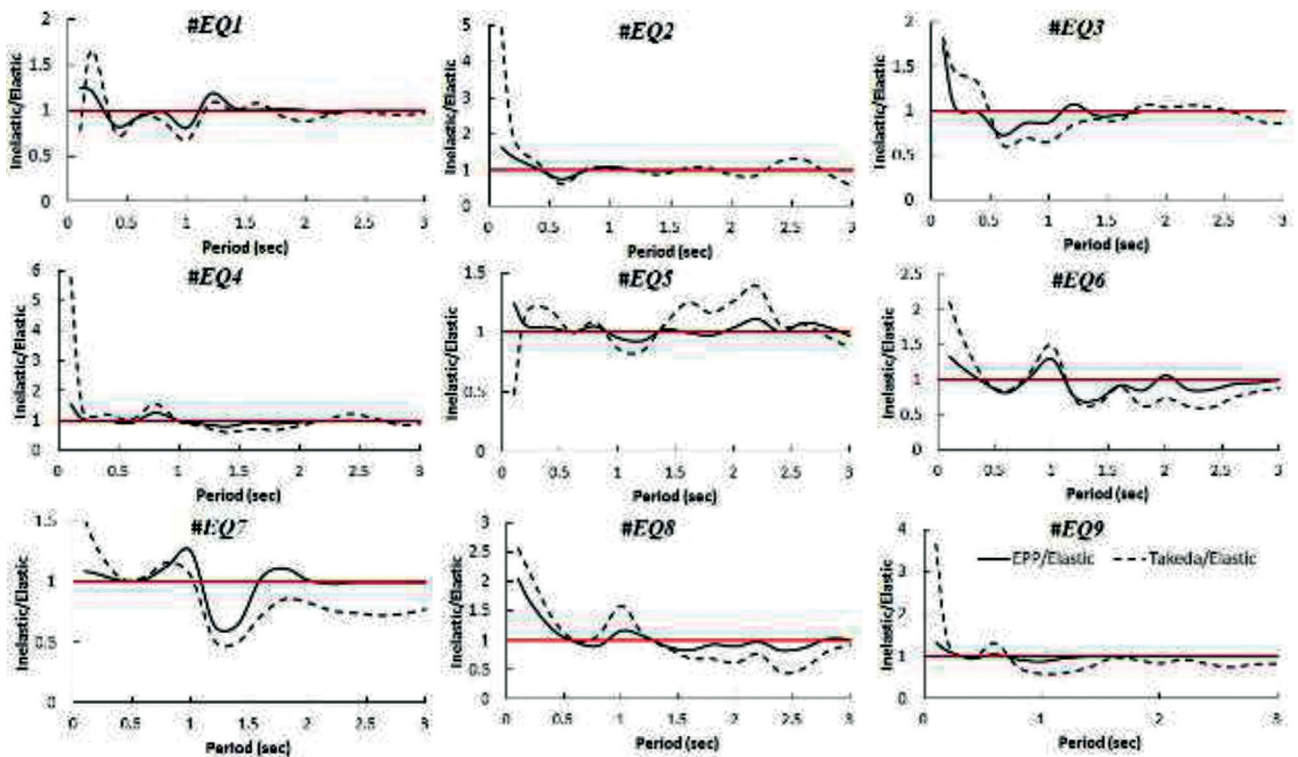
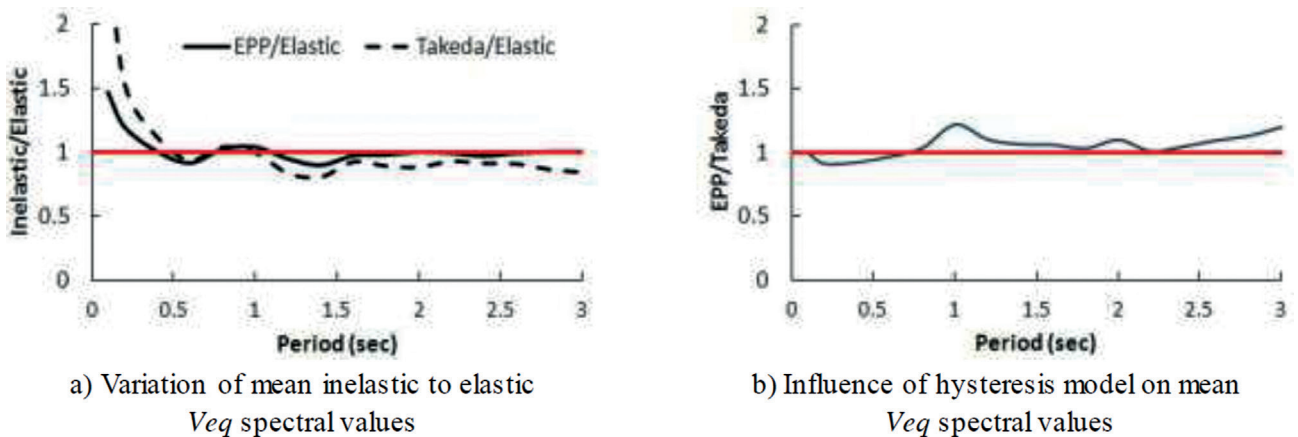


Figure 11. Ratios of inelastic to elastic  $V_{eq}$  spectral ordinates.



a) Variation of mean inelastic to elastic  $V_{eq}$  spectral values

b) Influence of hysteresis model on mean  $V_{eq}$  spectral values

Figure 12. Ratios of  $V_{eq}$  spectral ordinates computed for elastic and inelastic SDOF systems.

hysteresis model are greater than those of Modified Takeda hysteresis model.

**Variation of input energy spectral ordinates at different natural periods**

Input energy spectral values for SDOF systems having natural vibration periods of  $T_n = 0.2, 0.4,$  and  $0.6$  sec are presented in Table 2 in terms of energy equivalent velocity ( $V_{eq}$ ). For the period of  $T_n = 0.2$  sec, the computed spectral values of input energies of all GMs are higher for Modified Takeda hysteresis model. However, as the

natural period increases to  $T_n = 0.4$  and  $0.6$  sec, the difference in input energy spectral values between EPP and Modified Takeda models generally becomes smaller. The same trend is also observed at natural periods longer than  $0.6$  sec.

Input energy per unit mass spectral ordinates of the selected EQGMs are represented by bar charts in Figure 13 for both elastic and inelastic SDOF systems having natural vibration periods of  $T_n = 0.2, 0.4, 0.6, 0.8, 1.0,$  and  $1.2$  sec. The energy values are taken from the input energy spectra of Figures. 6, 7, and 8. These graphs may be considered

Table 2.  $V_{eq}$  (cm/sec) spectral ordinates for  $T_n = 0.2, 0.4$  and  $0.6$  sec

EQ No:	$T_n = 0.2$ sec			$T_n = 0.4$ sec			$T_n = 0.6$ sec		
	Elastic	EPP ( $\mu = 4$ )	Modified Takeda ( $\mu = 4$ )	Elastic	EPP ( $\mu = 4$ )	Modified Takeda ( $\mu = 4$ )	Elastic	EPP ( $\mu = 4$ )	Modified Takeda ( $\mu = 4$ )
#EQ1	27.63	33.52	45.97	51.00	42.11	38.29	37.60	35.04	35.97
#EQ2	5.91	7.98	11.31	12.51	13.05	15.11	22.61	17.19	14.04
#EQ3	11.62	12.13	16.73	24.70	24.43	32.25	43.91	32.14	27.66
#EQ4	9.47	9.92	12.40	22.45	22.15	27.04	35.76	32.77	36.04
#EQ5	19.42	20.62	22.45	20.18	21.16	24.07	23.46	23.54	23.37
#EQ6	10.10	11.99	16.57	22.42	21.57	22.95	28.51	23.13	23.83
#EQ7	27.92	29.92	35.77	31.66	32.18	32.72	30.54	31.19	31.76
#EQ8	3.22	5.35	6.91	13.56	16.03	18.56	21.95	21.22	21.79
#EQ9	11.00	12.44	14.57	16.25	15.59	15.36	12.32	12.96	16.21

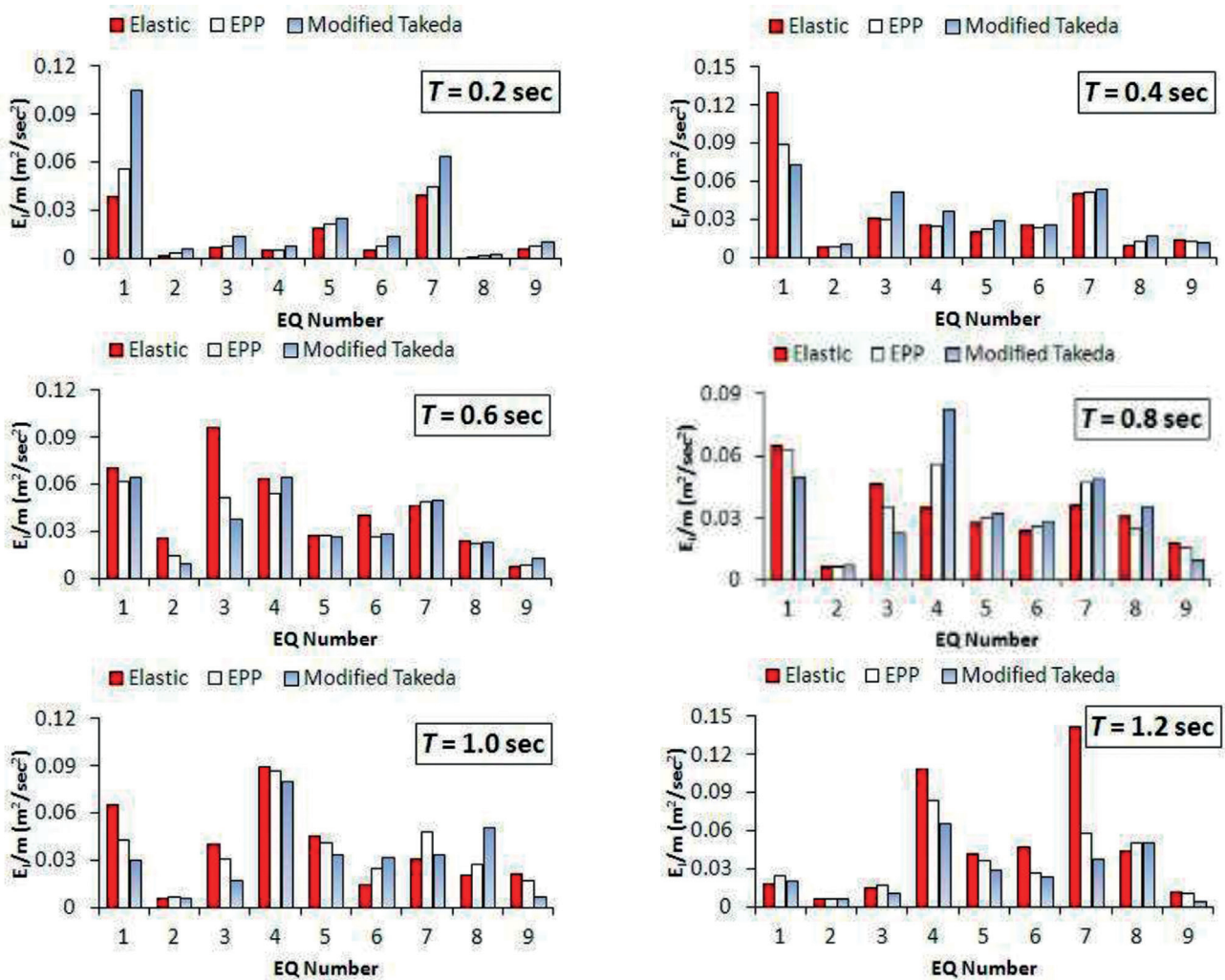
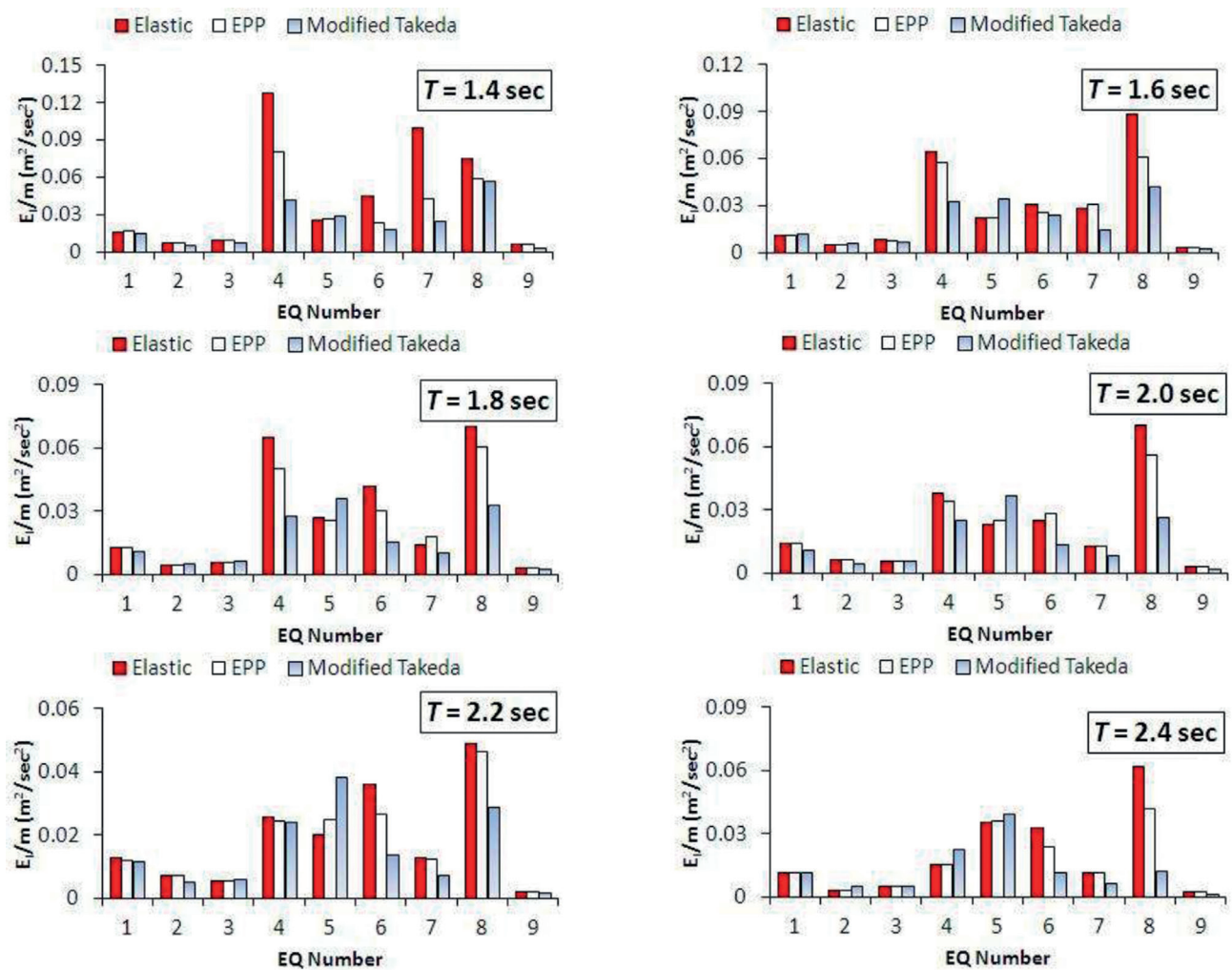


Figure 13.  $E_i/m$  spectral values at periods of 0.2, 0.4, 0.6, 0.8, 1.0 and 1.2 sec.

**Table 3.**  $V_{eq}$  (cm/sec) spectral ordinates for  $T_n = 0.8, 1.0$  and  $1.2$  sec

EQ No:	$T_n = 0.8$ sec			$T_n = 1.0$ sec			$T_n = 1.2$ sec		
	Elastic	EPP ( $\mu = 4$ )	Modified Takeda ( $\mu = 4$ )	Elastic	EPP ( $\mu = 4$ )	Modified Takeda ( $\mu = 4$ )	Elastic	EPP ( $\mu = 4$ )	Modified Takeda ( $\mu = 4$ )
#EQ1	36.05	35.54	31.67	36.11	29.20	24.51	18.76	22.29	20.38
#EQ2	11.39	11.32	11.93	10.54	11.56	11.24	11.38	11.37	11.56
#EQ3	30.54	26.63	21.41	28.47	24.93	18.69	17.27	18.63	14.57
#EQ4	26.56	33.46	40.76	42.29	41.65	40.10	46.61	40.92	36.30
#EQ5	23.37	24.62	25.35	30.09	28.73	25.85	29.05	26.98	24.33
#EQ6	21.82	22.54	23.89	17.06	22.17	25.44	30.83	23.14	21.93
#EQ7	26.94	30.64	31.40	24.71	31.10	25.98	53.30	34.11	27.48
#EQ8	24.72	22.33	26.75	20.18	23.48	31.93	29.71	31.68	31.81
#EQ9	18.85	17.54	14.00	20.69	18.34	12.18	14.92	14.44	9.16



**Figure 14.**  $E_i/m$  spectral values at periods of 1.4, 1.6, 1.8, 2.0, 2.2 and 2.4 sec.

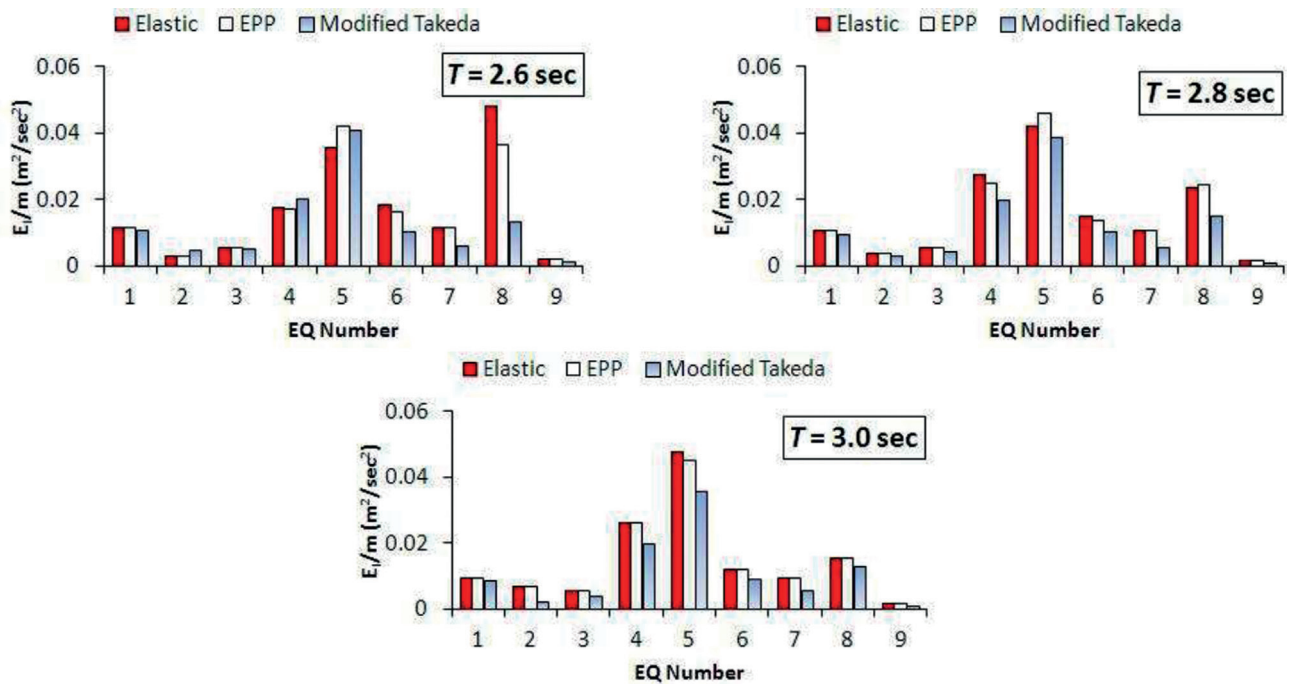


Figure 15.  $E_i/m$  spectral values at periods of 2.6, 2.8 and 3.0 sec.

Table 4.  $V_{eq}$  (cm/sec) spectral ordinates for  $T_n = 1.4, 1.6$  and  $1.8$  sec

EQ No:	$T_n = 1.4$ sec			$T_n = 1.6$ sec			$T_n = 1.8$ sec		
	Elastic	EPP ( $\mu = 4$ )	Modified Takeda ( $\mu = 4$ )	Elastic	EPP ( $\mu = 4$ )	Modified Takeda ( $\mu = 4$ )	Elastic	EPP ( $\mu = 4$ )	Modified Takeda ( $\mu = 4$ )
#EQ1	17.69	18.12	17.61	14.53	14.60	15.73	15.79	16.04	14.81
#EQ2	11.63	11.55	10.20	10.32	10.32	10.80	9.29	9.29	10.01
#EQ3	13.99	13.31	12.78	13.01	12.48	11.63	10.58	10.58	11.30
#EQ4	50.49	40.14	29.14	35.83	33.94	25.50	36.14	31.76	23.61
#EQ5	22.59	23.14	24.10	21.01	21.00	26.21	23.14	22.60	26.92
#EQ6	30.02	21.38	19.51	24.66	22.73	22.16	28.95	24.45	17.73
#EQ7	44.79	29.12	22.47	23.89	24.81	17.29	16.83	18.77	14.49
#EQ8	38.69	34.40	33.81	42.08	34.98	29.22	37.56	34.82	25.69
#EQ9	11.04	11.06	8.18	8.02	8.02	7.78	7.98	7.98	7.41

to be useful for variation of both elastic and inelastic input energy spectral values with the natural period of the system and GM characteristics.

In Table 3, input energy spectral values of SDOF systems having natural vibration periods of  $T_n = 0.8, 1.0,$  and  $1.2$  sec are presented in terms of equivalent velocity. As the period increases, it can be seen from the results of the study that the input energy difference between the elastic and inelastic systems becomes insignificant. Since all EQ records reflect their own amplitude, frequency, and duration characteristics to input energy computations, significant differences in seismic input energy can be observed

for individual EQGMs. It is noteworthy to point out that the selected records are unscaled (i.e., as recorded). As the natural period increases from  $T_n = 0.8$  to  $1.2$  sec, input energy spectral values of elastic systems become generally higher than that of the inelastic systems having hysteresis relations of EPP and Modified Takeda hysteresis model.

Input energy per unit mass spectral values of the selected EQGMs can be seen in Figure 14 for both elastic and inelastic SDOF systems having natural vibration periods of  $T_n = 1.4, 1.6, 1.8, 2.0, 2.2,$  and  $2.4$  sec, respectively. Input energy imposed on the elastic system is observed

**Table 5.**  $V_{eq}$  (cm/sec) spectral ordinates for  $T_n = 2.0, 2.2$  and  $2.4$  sec

EQ No:	$T_n = 2.0$ sec			$T_n = 2.2$ sec			$T_n = 2.4$ sec		
	Elastic	EPP ( $\mu = 4$ )	Modified Takeda ( $\mu = 4$ )	Elastic	EPP ( $\mu = 4$ )	Modified Takeda ( $\mu = 4$ )	Elastic	EPP ( $\mu = 4$ )	Modified Takeda ( $\mu = 4$ )
#EQ1	16.73	16.75	14.79	15.91	15.53	15.21	15.29	15.29	15.29
#EQ2	11.21	11.21	9.79	11.86	11.86	10.06	8.03	8.03	10.04
#EQ3	10.62	10.62	11.04	10.29	10.29	10.96	10.20	10.20	10.56
#EQ4	27.47	26.02	22.53	22.70	22.11	22.05	17.53	17.61	21.20
#EQ5	21.57	22.50	27.30	19.96	22.26	27.68	26.66	26.79	28.12
#EQ6	22.43	23.83	16.50	26.87	23.03	16.62	25.49	21.86	15.37
#EQ7	15.77	16.05	13.09	15.88	15.68	12.14	15.33	15.33	11.41
#EQ8	37.57	33.52	23.16	31.32	30.53	24.01	35.14	28.90	15.81
#EQ9	7.49	7.49	6.27	6.18	6.18	5.72	6.45	6.45	5.35

**Table 6.**  $V_{eq}$  (cm/sec) spectral ordinates for  $T_n = 2.6, 2.8$  and  $3.0$  sec

EQ No:	$T_n = 2.6$ sec			$T_n = 2.8$ sec			$T_n = 3.0$ sec		
	Elastic	EPP ( $\mu = 4$ )	Modified Takeda ( $\mu = 4$ )	Elastic	EPP ( $\mu = 4$ )	Modified Takeda ( $\mu = 4$ )	Elastic	EPP ( $\mu = 4$ )	Modified Takeda ( $\mu = 4$ )
#EQ1	15.07	15.07	14.63	14.47	14.47	13.81	13.61	13.61	13.25
#EQ2	7.62	7.62	9.86	8.56	8.56	7.66	11.66	11.66	6.40
#EQ3	10.52	10.52	10.27	10.50	10.50	9.27	10.60	10.60	9.10
#EQ4	18.64	18.57	20.10	23.45	22.32	20.01	22.84	22.78	19.93
#EQ5	26.76	29.01	28.58	28.96	30.35	27.91	30.82	29.97	26.74
#EQ6	19.20	18.02	14.31	17.30	16.59	14.30	15.41	15.39	13.60
#EQ7	15.09	15.09	10.93	14.67	14.67	10.78	13.56	13.56	10.53
#EQ8	31.01	27.04	16.37	21.64	22.15	17.53	17.45	17.60	16.12
#EQ9	6.62	6.62	4.94	5.75	5.75	4.70	5.47	5.47	4.54

to be higher than that imposed on the inelastic system at intermediate period ranges. However, input energy spectral ordinates are slightly different for linear elastic and inelastic systems at longer periods ( $T_n > 1.6$  sec). A similar trend is observed for the considered hysteresis models (i.e., the dependence on EPP hysteresis model is almost lost at longer periods).

Input energy per unit mass spectral values of selected EQGMs can be seen from Fig. 15 for both elastic and inelastic SDOF systems having natural vibration periods of  $T_n = 2.6, 2.8,$  and  $3.0$  sec, respectively. For long period systems, it is seen from the study that input energies spectral ordinates are obtained quite close to each other for elastic and inelastic systems.

Input energy spectral values computed for SDOF systems having natural vibration periods of  $T_n = 1.4, 1.6,$  and  $1.8$  sec are presented in Table 4 in terms of equivalent velocity. As the period increases from  $T_n = 1.4$  sec to  $T_n = 1.8$  sec, it can be seen from the results that the energy difference

between elastic and inelastic systems is not significant. The results in Table 4 show that the difference between input energy spectral ordinates of elastic and inelastic systems is quite small and they are observed to become closer as the period elongates.

In Table 5, input energy spectral values of SDOF systems having natural vibration periods of  $T_n = 2.0, 2.2,$  and  $2.4$  sec are presented in terms of energy equivalent velocity. Finally, energy equivalent velocity spectral ordinates are presented in Table 6, for relatively longer periods of  $T_n = 2.6, 2.8,$  and  $3.0$  sec. It is quite clear that inelastic behaviour has almost no significant influence on seismic input energy spectral values of relatively long-period systems.

## CONCLUSIONS

Input energy spectra of far-fault GMs are computed for linear elastic systems and inelastic systems. EPP and

Modified Takeda hysteresis models are considered in nonlinear modeling of SDOF systems. GMs are selected to have the closest fault distances are more than 30 km and they do not have any impulsive characteristics. Time history analyses have been performed using selected EQs for SDOF systems having a damping ratio of 5%. A constant ductility ratio of  $\mu = 4$  is considered for the inelastic models. The main findings of the study can be sorted as below:

- Elastic and inelastic input spectra of far-field GMs are somewhat different and hysteresis model has some influence on inelastic input spectra at different period ranges.
- Input energy demand imposed on inelastic systems is greater than that of elastic systems at short periods ( $T < 0.5$  sec). However, elastic input energy becomes higher than inelastic input spectra at intermediate and long periods.
- Far-fault input energy spectra have some dependency on hysteresis model along the entire period range. However, inelastic input spectra of SDOF system simulated by EEP hysteresis model is found to be very close to elastic input spectra at long periods. At short periods hysteresis model is found to be more influential on inelastic input energy spectra.
- Elastic and inelastic input energy spectra of EQ7, EQ8, and EQ9 which are recorded during the same event but at different stations are not the same. At short periods  $V_{eq}$  spectral values are greater for EQ7 which has the smallest distance between them. However, at longer periods this trend is no longer valid.
- Input energy spectra for inelastic systems have no significant dependency on hysteresis models, especially for intermediate and long period systems. However, the number of the selected GMs is very limited and the variation of different parameters such as yield strength, post-yield stiffness factor, unloading, and reloading stiffness used to define hysteresis rules is not taken into consideration. Accordingly, the results of the present study are valid for only the considered hysteresis models and the selected EQGMs.

#### AUTHORSHIP CONTRIBUTIONS

Authors equally contributed to this work.

#### DATA AVAILABILITY STATEMENT

The authors confirm that the data that supports the findings of this study are available within the article. Raw data that support the finding of this study are available from the corresponding author, upon reasonable request.

#### CONFLICT OF INTEREST

The author declared no potential conflicts of interest with respect to the research, authorship, and/or publication of this article.

#### ETHICS

There are no ethical issues with the publication of this manuscript.

#### REFERENCES

- [1] UBC. Uniform building code, International Conference of Building Officials Officials, Whittier, California, USA, 1997.
- [2] CEN. Eurocode 8: Design of structures for earthquake resistance - Part 1: General rules, seismic actions and rules for buildings, European Committee for Standardization, Brussels, Belgium, 2004.
- [3] NBCC. National building code of Canada, associate committee on the national building code, National Research Council of Canada, Ottawa, Ontario, 2005.
- [4] IBC. International building code, International Code Council, Country Club Hills, Illinois, USA, 2006.
- [5] ASCE. Minimum design loads for buildings and other structures, ASCE/SEI Standard 7-10, USA, 2010
- [6] TBEC. Turkey building earthquake code, The Disaster and Emergency Management Presidency of Turkey, Ankara, Turkey, 2018.
- [7] Priestley MJN, Calvi GM, Kowalsky MJ. Displacement-based seismic design of concrete structures, Sixth National Conference on Earthquake Engineering, Istanbul, Turkey, 16-20 October, 2007.
- [8] Priestley MJN, Calvi GM, Kowalsky MJ. Displacement based seismic design of structures. IUSS Press: Pavia, Italy, 2007.
- [9] Akbaş B, Shen J. Energy approach in performance-based earthquake resistant design (PB-EQRD), 12th European Conference on Earthquake Engineering, Paper Reference 043, London, UK, 2002.
- [10] Uang CM, Bertero V. Evaluation of seismic energy in structures. *Earthq Eng Struct Dyn* 1990;19:77–90. [\[CrossRef\]](#)
- [11] Fajfar P, Fischinger MA. Seismic procedure including energy concept, Ninth European Conference on Earthquake Engineering (ECEE), Moscow, 1990.
- [12] Akbaş B, Shen J. Earthquake-resistant design (EQRD) and energy concepts. *IMO Teknik Dergi*, 2003;192:2877–2901 [Turkish]
- [13] Dindar AA, Yalçın C, Yüksel E, Özkaynak H,

- Büyüköztürk O. Development of earthquake energy demand spectra. *Earthq Spectra* 2015;31:1667–1689. [CrossRef]
- [14] Sucuoğlu H, Alici FS. Elastic and inelastic near fault input energy spectra, COMPDYN 2019 7th ECCOMAS Thematic Conference on Computational Methods in Structural Dynamics and Earthquake Engineering, Crete, Greece, 24-26 June, 2019. [CrossRef]
- [15] Housner GW. Limit design of structures to resist earthquakes, Proceedings of the 1st World Conference on Earthquake Engineering, Oakland, California, USA, 1956.
- [16] Akiyama H. Earthquake-Resistant Limit-State Design for Buildings. Tokyo: University of Tokyo Press; 1985.
- [17] Kuwamura H, Galambos TV. Earthquake load for structural reliability. *J Struct Eng* 1989;115:1446–1462. [CrossRef]
- [18] Fajfar P, Vidic T, Fischinger M. Seismic demand in medium-and long-period structures. *Earthq Eng Struct Dyn* 1989;18:1133–1144. [CrossRef]
- [19] Manfredi G. Evaluation of seismic energy demand. *Earthq Eng Struct Dyn* 2001;30:485–499. [CrossRef]
- [20] Benavent-Climent A, Pujades LG, López-Almansa F. Design energy input spectra for moderate seismicity regions. *Earthq Eng Struct Dyn* 2002;31:1151–1172. [CrossRef]
- [21] Khashaei P. Energy-based seismic design and damage assessment for structures. Doctorial Dissertation. Dallas, Texas: Southern Methodist University; 2004.
- [22] López-Almansa F, Yazgan AU, Benavent-Climent A. Design energy input spectra for high seismicity regions based on Turkish registers. *Bull Earthq Eng* 2013;11:885–912. [CrossRef]
- [23] Donaire-Ávila J, Benavent-Climent A, Lucchini A, Mollaioli F. Energy-based seismic design methodology: A preliminary approach, 16th World Conference on Earthquake Engineering (16WCEE), 9-13 January, Santiago, Chile, 2017.
- [24] Zhou Y, Song G, Huang S, Wu H. Input energy spectra for self-centering SDOF systems. *Soil Dyn Earthq Eng* 2019;121:293–305. [CrossRef]
- [25] Erduran E. Hysteretic energy demands in multi-degree-of-freedom systems subjected to earthquakes. *Build* 2020;10:220:1–17. [CrossRef]
- [26] Cheng Y, Dong Y-R, Quin L, Wang Y-Y, Li Y-X. Seismic energy response of SDOF systems subjected to long-period ground motion records. *Adv Civil Eng* 2021;6655400. [CrossRef]
- [27] Gullu A, Yuksel E, Yalcin C, Buyukozturk O. Damping effect on seismic input energy and its verification by shake table tests. *Adv Struct Eng* 2021;24:2669–2683. [CrossRef]
- [28] Merter O. An investigation on the maximum earthquake input energy for elastic SDOF systems. *Earthq Struct* 2019;16:487–499.
- [29] Fajfar P, Vidic T. Consistent inelastic design spectra: Hysteretic and input energy, *Earthq Eng Struct Dyn* 1994;23:523–537. [CrossRef]
- [30] Chopra AK. Dynamics of structures. Theory and applications to earthquake engineering, New Jersey: Prentice Hall; 2015.
- [31] Riddell R, Garcia JE. Hysteretic energy spectrum and damage control. *Earthq Eng Struct Dyn* 2001;30:1791–1816. [CrossRef]
- [32] Mezgebo M, Lui EM. Hysteresis and soil site dependent input and hysteretic energy spectra for far-source ground motions. *Adv Civil Eng* 2016;1:1–29. [CrossRef]
- [33] Uçar T, Merter O. Variation of energy input to non-linear single degree of freedom system with period and ductility ratio. 4th International Conference on Earthquake Engineering and Seismology (4. ICEES), Eskişehir, Turkey, 11-13 October, 2017.
- [34] PEER. Pacific Earthquake Engineering Research Center Strong Ground Motion Database, Available at: <https://ngawest2.berkeley.edu/> (Accessed on Sept 05, 2022).
- [35] Takeda T, Sozen MA, Nielsen NN. Reinforced concrete response to simulated earthquakes. *J Struct Div* 1970;96:2557–2573. [CrossRef]
- [36] Otani S. SAKE: A computer program for inelastic response of RC frames subject to earthquakes, Civil Engineering Studies Technical Report-SRS-413, University of Illinois, Urbana, 1974.
- [37] PRISM for Earthquake Engineering. A software for seismic response analysis of single-degree-of-freedom systems, Department of Architectural Engineering, INHA University, 2011.
- [38] Alici FS, Sucuoğlu H. Elastic and inelastic near-fault input energy spectra. *Earthq Spectra* 2018;34:611–637. [CrossRef]
- [39] Ucar T. Computing input energy response of MDOF systems to actual ground motions based on modal contributions. *Earthq Struct* 2020;18:263–273. [CrossRef]
- [40] Decanini LD, Mollaioli F. An energy-based methodology for the assessment of seismic demand. *Soil Dyn Earthq Eng* 2001;21:113–137. [CrossRef]